

DOI: 10.17148/IJIREEICE.2025.131020

An Improved Control Strategy for Bidirectional Wireless Power Transfer in Grid-to-Vehicle and Vehicle-to-Home Applications Using a Fuzzy Logic Controller

SURAVARJALA PRADEEP SAI TEJA¹, CH. VISHNU CHAKRAVARTHI²

PG Student, Department of Electrical Engineering, Sankethika Vidya Parishad Engineering College, Andhra Pradesh, India¹

Assistant Professor, Department of Electrical Engineering, Sankethika Vidya Parishad Engineering College,

Andhra Pradesh, India²

Abstract: The progress in the charging strategies for electric vehicles is expected to have significant impacts on the electric grid in the near future. Electric vehicle battery chargers are designed to facilitate bidirectional power transfer in accordance with the vehicle-to-grid concept, thereby providing essential services to both the distribution grid and the domestic grid of the vehicle owner. Wireless power transfer battery chargers present a safer and more user-friendly option for individuals who may lack confidence in handling technological devices. Bidirectional wireless power transfer chargers that support vehicle-to-grid services represent a natural progression of the previously mentioned concepts. This paper addresses the development of a control strategy for such a battery charger, concentrating on the requirements of the power conversion stages necessary for the operation of a charger designed for vehicle-to-home functionality. Initially, the division of the control strategy into two distinct levels is discussed, followed by an introduction to the interaction between the algorithms at the internal and external levels. In the implementation of the control algorithms, the decision was made to design the controllers with simplicity in mind. This approach allowed for the adoption of well-established techniques within the scientific community for their design, while also minimizing the computational resources required for their execution. Despite the straightforward nature of the controllers, the introduction and management of interactions among the various algorithms resulted in the formulation of a comprehensive control strategy that simultaneously adheres to the voltage and current limits imposed by the grid and the battery, while also preventing the maximum operating conditions of the static converters that comprise the system from being exceeded. The algorithms and their corresponding controllers are developed sequentially in the continuous time domain, utilizing techniques grounded in the analysis of Bode diagrams of the transfer functions integral to the system's operation. In the design of the controllers, the implications of their subsequent effects are also taken into account.

I. INTRODUCTION

In light of the prevailing trends in technological progress, electric vehicles (EVs) are being proposed as a future transportation solution that offers energy efficiency and aids in the reduction of greenhouse gas emissions. The Global EV Outlook 2021 indeed indicates that the projected sales of light-duty vehicles are expected to increase from 3 million in 2020 to 25 million by 2030 [1]. Within this context, EVs present a challenge regarding power demand for the grid system. Fortunately, this challenge can be addressed by the EVs themselves, utilizing their batteries as energy sources to support the grid [2], [3]. Traditional battery chargers facilitate energy transfer through a plug and socket connection. Plug-in charging encounters issues related to electrical insulation, can be inconvenient during adverse weather conditions such as rain, snow, or ice, and may raise concerns among individuals who are not familiar with electrical devices. Currently, wireless power transfer (WPT) technology provides an alternative method for charging EVs. In comparison to its wired equivalent, WPT technology offers numerous advantages, including built-in isolation and shock prevention, fewer complications arising from moisture and dirt, increased flexibility, lower maintenance requirements, and enhanced userfriendliness [4], [5]. The traditional battery chargers facilitate energy transfer via a plug and socket combination. Plug-in charging encounters challenges related to electrical insulation, can be inconvenient during adverse weather conditions such as rain, snow, or ice, and may raise concerns among individuals who are not familiar with electrical devices. In contemporary times, wireless power transfer (WPT) technology presents an alternative method for charging electric vehicles (EVs). In comparison to wired charging systems, WPT technology offers numerous advantages, including builtin isolation and shock prevention, reduced complications from moisture and dirt, increased flexibility, lower maintenance



DOI: 10.17148/IJIREEICE.2025.131020

requirements, and enhanced user-friendliness [4], [5]. The primary drawbacks of WPT battery chargers are their comparatively lower efficiency relative to conventional chargers and the electromagnetic emissions near the coupling coils [6]. Nevertheless, these concerns are not particularly significant, especially for static applications like the one discussed in this paper. With meticulous coil design, the average efficiency during battery charging can easily surpass 90% [7], while the vehicle's chassis serves as a natural shield against electromagnetic fields [8]. It is widely recognized that vehicles are typically parked for the majority of the day. This situation allows for battery charging during periods of low power demand from the grid, a process known as power shaving. If battery chargers are capable of managing bidirectional power flow, EVs can function both as a load and as an energy source for the grid [9]. In fact, they can return stored energy during peak demand periods, provided that the battery's state of charge is replenished before the EVs are utilized [10], [11], [12], [13]. Electric vehicles can assist the grid by alleviating fluctuations in available power associated with renewable energy sources or by regulating grid frequency [14], [15], [16]. In addition to the benefits for the grid, utilizing EV batteries can provide economic returns for their owners. This power exchange method is referred to as vehicle to grid (V2G) [17], [18]. The V2G strategy can also be implemented on a smaller scale to balance and meet household energy requirements through smart EV battery charging. This specific application of V2G is termed vehicle to home (V2H) [19], [20], [21], [22]. A typical V2H configuration is illustrated in Fig. 1. The V2H method assists in reducing the daily variable load demand of household appliances, for instance, by charging the EV battery overnight when domestic power consumption is lower. During daytime, the stored energy can be fed back into the domestic grid whenever energy demand rises [23], [24], [25], [26]. This paper intends to thoroughly outline the control strategy for a bidirectional wireless battery charger with V2H functionality (BWV2H) [2]. The strategy is crafted to meet the grid's requirements regarding maximum exchanged power, as well as the battery's specifications concerning charging and discharging currents and voltages. Simultaneously, the voltages of the dc buses in both sections of the BWV2H are kept from surpassing their designated operating voltages. The comprehensive strategy includes eleven distinct control algorithms arranged in two levels that function in a coordinated fashion. The internal level comprises four algorithms that directly interact with the individual static converters that constitute the BWV2H. The external level includes seven algorithms that produce the references for the internal level algorithms and ensure the consistent operation of the primary and secondary sections of the BWV2H. These seven algorithms are categorized into three groups: three are always active, two are activated solely during battery charging, and two function exclusively during battery discharge.

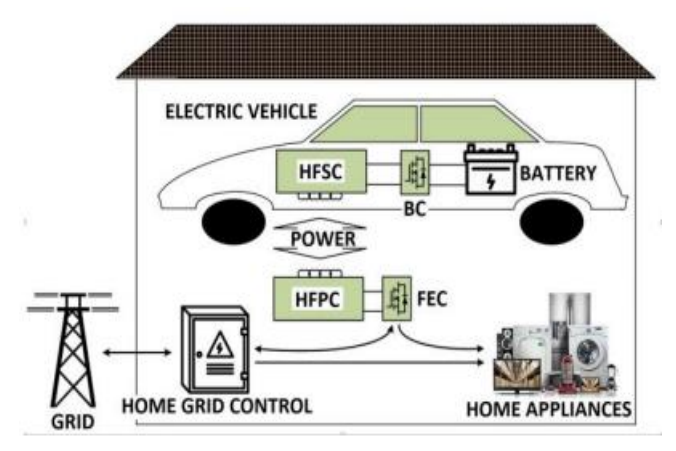


Figure 1. BWV2H in the home grid

Each algorithm is based on a straightforward PI type controller, yet their precisely engineered interactions enable the system to function correctly under all operating conditions, facilitating a smooth transition from one condition to another without necessitating more complex solutions. The sizing procedure for each controller is thoroughly detailed, equipping readers with the knowledge to design their own BWV2H control system based on its parameters. Numerous papers in the literature address this subject; however, most concentrate on a singular aspect of the issue, typically the management of the WPT sub-system, while overlooking the necessity to also manage interactions with the grid and the EV battery. Additionally, highly sophisticated control algorithms are frequently introduced without providing adequate information for readers to replicate the published results in their own prototypes. For instance, references [27] and [28] examine the power exchange between the EV battery and another battery located in the house, yet they completely disregard the interaction with the grid and the associated issues. Similarly, there is no description of any control algorithm. Like the previous paper, reference [11] focuses solely on the power transfer between the dc buses of the BWV2H, failing to address battery and grid limitations and not explaining regulator sizing. Furthermore, it appears that only one microprocessor is utilized to control both sections of the system. Paper [29] exclusively discusses the power exchange between the two sections of the BWV2H, employing a predictive controller; however, it does not consider the interface with the grid, nor does it provide explanations regarding



DOI: 10.17148/IJIREEICE.2025.131020

the generation of the power reference. Grid interfacing is also not addressed in [30], and the proposed control algorithm does not transition smoothly from constant current to constant voltage battery charging.

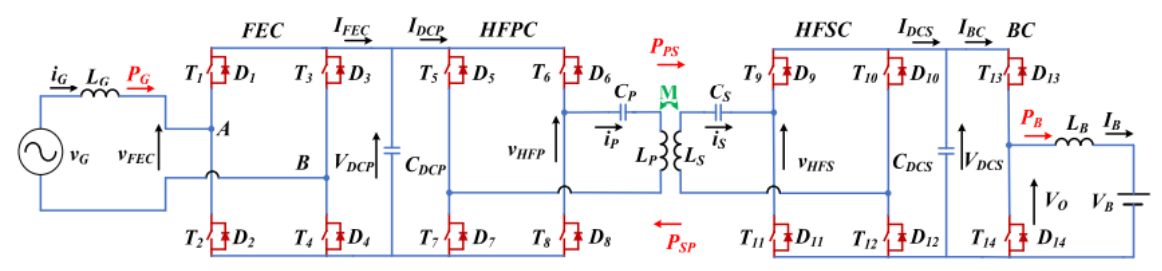


Figure 2. Circuit scheme of the BWV2H.

Action carried out	Name	Controlled quantity	Manipulated quantity	Level	Active	Controller's TF	Subsection
Grid current control	AL_i _G _B	i_G	V_{FEC}	Internal	Both	C _{iG,VFEC} (s)	IV.B.1
Secondary coil current control	$AL_I_s_C$	I_S	V_{HFP}	Internal	Charge	$C_{IS,VHFP}(s)$	IV.B.2
Primary coil current control	$AL_{I_P}D$	I_P	V_{HFS}	Internal	Discharge	$C_{IP,VHFS}(s)$	IV.B.3
Battery current control	$AL_{I_B}B$	I_B	V_0	Internal	Both	$C_{IB,VO}(s)$	IV.B.4
V _{DCP} voltage regulation	$AL_V_{DCP}B$	V_{DCP}	$P_G(i_G)$	External	Both	$C_{VDCP,PG}(s)$	IV.C.1
V _{DCP} voltage regulation	$AL_V_{DCP}C$	V_{DCP}	$P_{PS}(I_S)$	External	Charge	$C_{VDCP,PPS}(s)$	IV.C.2
V _{DCP} voltage regulation	$AL_V_{DCP}D$	V_{DCP}	$P_{SP}(I_P)$	External	Discharge	$C_{VDCP,PSP}(s)$	IV.C.3
V _{DCS} voltage regulation	$AL_V_{DCS}B$	V_{DCS}	$P_B(I_B)$	External	Both	$C_{VDCS,PB}(s)$	IV.C.4
V _{DCS} voltage regulation	$AL_V_{DCS}_C$	V_{DCS}	$P_{PS}(I_S)$	External	Charge	$C_{VDCS,PPS}(s)$	IV.C.5
V _{DCS} voltage regulation	$AL_V_{DCS}D$	V_{DCS}	$P_{SP}(I_P)$	External	Discharge	$C_{VDCS,PSP}(s)$	IV.C.6
V _B voltage regulation	$AL_V_B_B$	V_B	$P_B(I_B)$	External	Both	$C_{VB,PB}(s)$	IV.C.7

Table 1. Control Algorithms of the BWV2H.

The paper [31] also addresses the subject of connecting the primary side DC bus to the grid, but it is restricted to the necessity of sustaining a constant DC voltage, without considering the limitations of grid power. Similarly, the control algorithm for the secondary section oversees the power transfer but relies on an external control loop, which is not discussed in the paper, for managing battery charging. In [32], the challenge of power exchange with the grid is tackled, and the control of the proposed matrix converter is elaborated upon; however, the interaction with the battery is not examined in depth. Like the previous study, [33] primarily concentrates on the exchange of active and reactive power with the grid, yet it lacks detailed information regarding battery charge management and the design of the associated controller. The BWV2H discussed in this paper [2] has been developed by adhering closely to the guidelines set forth in the SAE J2954 report [34], which only considers unidirectional WPT systems. The power rating and the interface requirements with the grid have been derived from the Italian technical standards (CEI 0-21) [35]. Specifically, the paper is structured as follows: Section II outlines the circuit scheme and operational principles of the static converters that constitute the BWV2H. Section III details the overall control strategy of the battery charger, defines the roles of the various control algorithms, and examines the mechanisms and implications of their interactions. Section IV provides a comprehensive overview of the development of the individual control algorithms, including the block diagram of the complete control loop for each algorithm and the results of preliminary simulations conducted to validate their proper functioning. Section V focuses on verifying the operation of the complete control strategy, addressing both battery charging and discharging, and offers a thorough description of the different operational modes of the BWV2H during these two processes. Section VI concludes the paper.

II. CIRCUITAL SCHEME OF THE BWV2H

Figure 2 illustrates the circuit diagram of the BWV2H. In this diagram, as well as throughout the entire paper, uppercase letters represent constant values or values that change slowly in relation to the grid frequency, peak amplitudes of alternating values, or average values of continuous quantities. Conversely, lowercase letters denote alternating or variable quantities that occur at or above the grid frequency. The BWV2H connects to the domestic grid via the front-end converter (FEC), which is fitted with an inductive input filter referred to as LG. The FEC draws the current iG from the domestic grid. The phase of iG in relation to the grid voltage vG is modified to establish the direction of active power flow and the extent of reactive power exchanged with the grid, if applicable. At the output of the FEC, the capacitor CDCP maintains the dc bus of the primary section. The continuous voltage VDCP, which can be regarded as nearly constant, is supplied to the input of the high-frequency primary converter (HFPC). The HFPC produces a quasi-square wave voltage vHFP at a nominal supply frequency of 85 kHz [34], and regulates the first harmonic amplitude VHFP of this voltage by modifying the phase delay between the gate signals of its two legs, in accordance with the phase shift control technique [36]. The



DOI: 10.17148/IJIREEICE.2025.131020

HFPC powers the primary coil and its compensation network, which includes the capacitor CP connected in series with the coil and resonating with the coil's self-inductance [34], [37]. Due to resonance, the current iP flowing through the primary coil is nearly sinusoidal. This current generates a variable magnetic induction flux that connects with the secondary coil, inducing an alternating voltage across its terminals. The induced voltage serves as the means for transferring power PPS from the primary to the secondary section of the BWV2H. The series resonant capacitor CS compensates for the voltage drop caused by the current iS flowing through the self-inductance LS of the secondary coil. As a result, the first harmonic of the voltage vHFS applied at the input of the high-frequency secondary converter (HFSC) is ideally equal to the induced voltage. During the charging process, the switches T9-T12 of the HFSC remain inactive, allowing the current iS to pass through the freewheeling diodes. The alternating component of the rectified current IDCS flows into the capacitor CDCS. The average component of IDCS, referred to as IBC, is appropriately conditioned by the bidirectional chopper (BC), which generates the current IB that charges the battery. The capacitor CDCS is designed to ensure that the dc bus voltage VDCS of the secondary section of the BWV2H remains constant. Assuming that iS flows alternately across the pairs of diodes D9-D12 and D10-D11 for the entire supply period, it follows from the constant value of VDCS that vHFS indeed exhibits a square waveform.

To reverse the direction of power flow, that is, to transfer the power PSP from the EV battery to the grid, it is adequate to modify the current references supplied to the control loops of FEC and BC, as well as to interchange the control strategies of HFPC and HFSC. Consequently, the HFPC functions as a high-frequency diode rectifier, while the HFSC acts as a high-frequency inverter.

III. CONTROL STRATEGY OF THE BWV2H

The control strategy established for the BWV2H is based on a series of control algorithms that work together to ensure the system operates under the necessary conditions. The names and characteristics of these algorithms are outlined in Table 1. Each algorithm is labeled as 'AL X Y', where 'AL' signifies 'algorithm', 'X' represents the controlled quantity, and 'Y' indicates when the algorithm is activated, i.e., during battery charging ('C'), discharging ('D'), or both operations ('B'). Each control algorithm regulates one quantity by adjusting another. The transfer function (TF) of the controller created for each algorithm is represented as CX,Z(s), where X denotes the controlled quantity and Z the manipulated one. Their names are provided in the second to last column of Table 1. The algorithms are categorized into two tiers: internal and external. The quantities manipulated by the external level algorithms serve as indirect references for the quantities controlled by the internal level algorithms. The external level algorithms manage the voltages of the two DC buses and the battery. To achieve this, they produce references for the power PPS and PSP, which are exchanged between the two sections of the BWV2H, for the power PB that is supplied to the battery, and for the power PG that is drawn from the grid. The internal level algorithms are tasked with controlling the currents iG, IB, and the amplitudes IP and IS of the currents iP and iS. Consequently, the power references generated by the external level are adjusted using straightforward relationships to transform them into the current references needed by the internal level algorithms. These current references are indicated within parentheses in Table 1. The internal algorithms at the level of operation calculate the references for the voltages vFEC, vHFP, vHFS, and VO that are required to be produced by the static converters that make up the BWV2H.

The always-on algorithms AL VB B, AL VDCS B, and AL VDCP B are specifically tasked with managing the voltages across the battery and the capacitors CDCS and CDCP. The first two algorithms adjust the power PB exchanged with the battery, while the third one regulates the power PG drawn from the grid. The algorithms AL VDCS C and AL VDCP C are operational during the battery charging phase. They maintain the voltages across the capacitors CDCS and CDCP at a steady value by influencing PSP through the amplitude IS of iS. Conversely, the algorithms AL VDCS D and AL VDCP D are engaged during the battery discharging process and oversee the same voltages VDCS and VDCP, but they do so by acting on PSP via IP. The operations of the algorithms that are triggered during battery charging or discharging coincide with those of the two always-on algorithms that produce the references for PB and PG. For instance, during the battery charging phase, both AL VDCS B and AL VDCS C regulate VDCS by adjusting PB and PPS through IB and IS. In a practical application, a battery management system regulates the battery voltage during charging and monitors it during discharging. However, to finalize the design of the control strategy for the BWV2H and to simulate its operation under all working conditions, the subsequent discussion assigns the functions of the battery management system to AL VB B. By adjusting IB, it ensures that the battery is initially charged at a constant current and subsequently at the constant voltage specified by the manufacturer. Furthermore, it ensures that the battery is discharged without surpassing the maximum current and minimum voltage. The implementation of the internal level algorithms necessitates the transduction and acquisition of the currents iG, iP, iS, and IB. Additionally, the grid voltage vG must be transduced to facilitate the control of the phase of the current iG. The external level algorithms require the transduction and acquisition of the voltages VB, VDCS, and VDCP. The signals obtained from the circuitry that transduces IB, ig, vg, VB, VDCS, and VDCP are processed by an analog low pass filter (LPF). Ultimately, they are acquired by the microcontrollers that execute the control strategy.



DOI: 10.17148/IJIREEICE.2025.131020

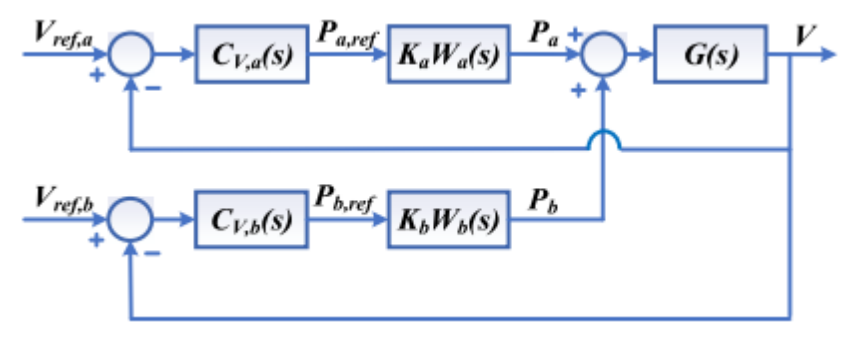


Figure 3. Block diagram of interaction of first between two control Loops.

The subsections pertaining to the design of the various controllers are detailed in the last column of Tab. 1.

IV. CONTROL ALGORITHMS DESIGN

To verify the effectiveness of the overall control strategy, the control algorithms detailed in the preceding sections have been implemented in two distinct simulation models: one for battery charging and the other for discharging. To enhance the speed of the simulations, the control loops of iG and IB have been represented through their transfer functions (TFs). Conversely, the control loops of IP and IS, along with VDCP, VDCS, and VB, have been simulated using the block diagram presented in the corresponding subsections. This is due to their interdependent interactions, which could not be accurately modeled by solely considering the resultant TFs. The HFPC and HFSC have been represented by a delay corresponding to their switching periods, while the TFs between vHFS and IP, as well as between vHFP and IS, have been modeled using the gain KVHFP,IS as specified in equation (26).

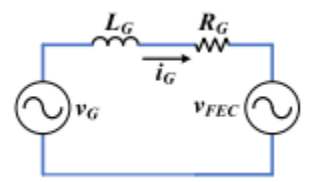


Figure 4. Equivalent scheme of the system to be controlled.

Consistent with the previous section, the battery has been modeled as a capacitor in series with a resistor. The maximum integration step for these simulations has been established at $10 \, \mu s$. Appendix B contains the simplified flow charts pertinent to the implementation of the control strategy in the two sections of the BWV2H during both the charging and discharging phases of the battery.

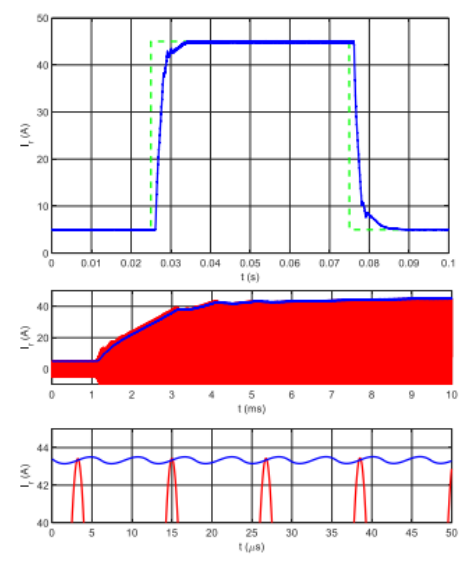


Figure 5. AL_IS _C responses. Top: IS,ref (dashed green) and IS (blue). Bottom: iS (red) and IS (blue) during transient and their magnifications.





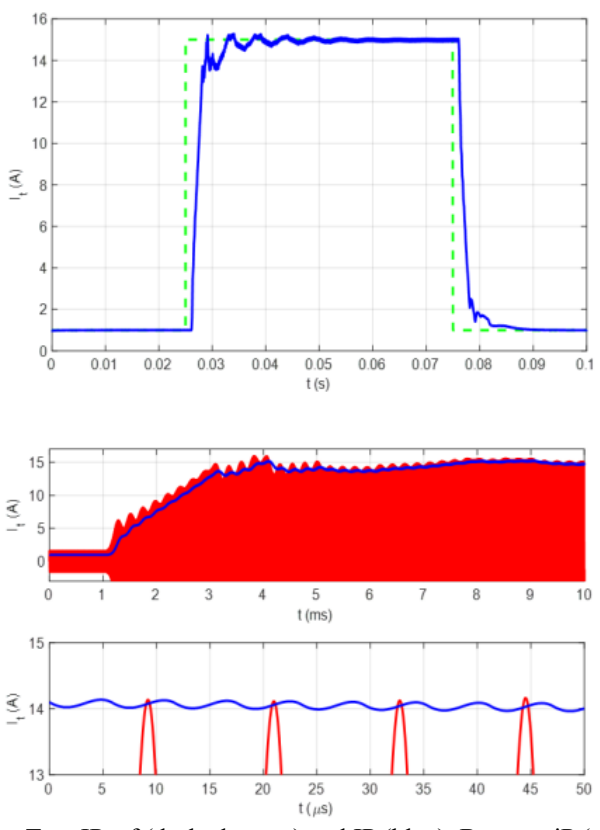


Figure 6. AL_IP_D responses. Top: IP,ref (dashed green) and IP (blue). Bottom: iP (red) and IP (blue) during transient and their magnifications.

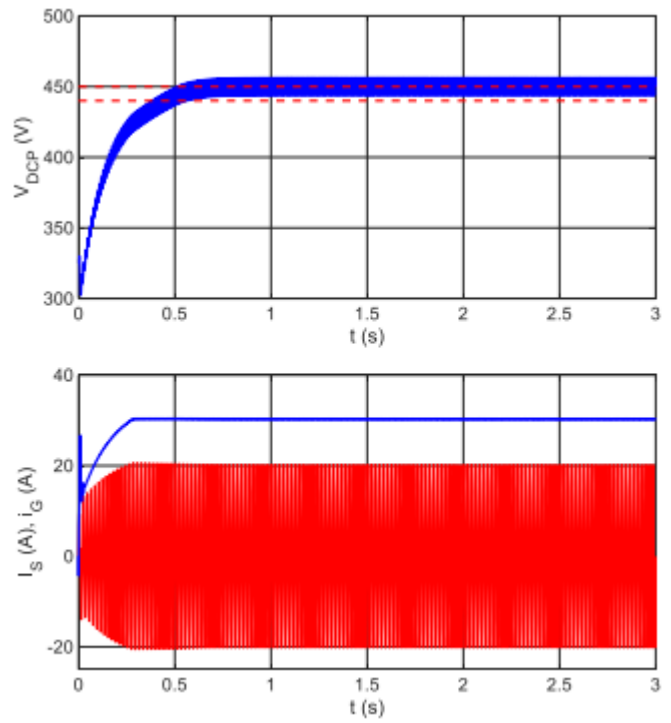


Figure 7. Top: Voltage VDCP (blue), VDCP,ref,high (dashed red), and VDCP,ref,low (dashed red). Bottom: IS (blue) and iG (red).



DOI: 10.17148/IJIREEICE.2025.131020

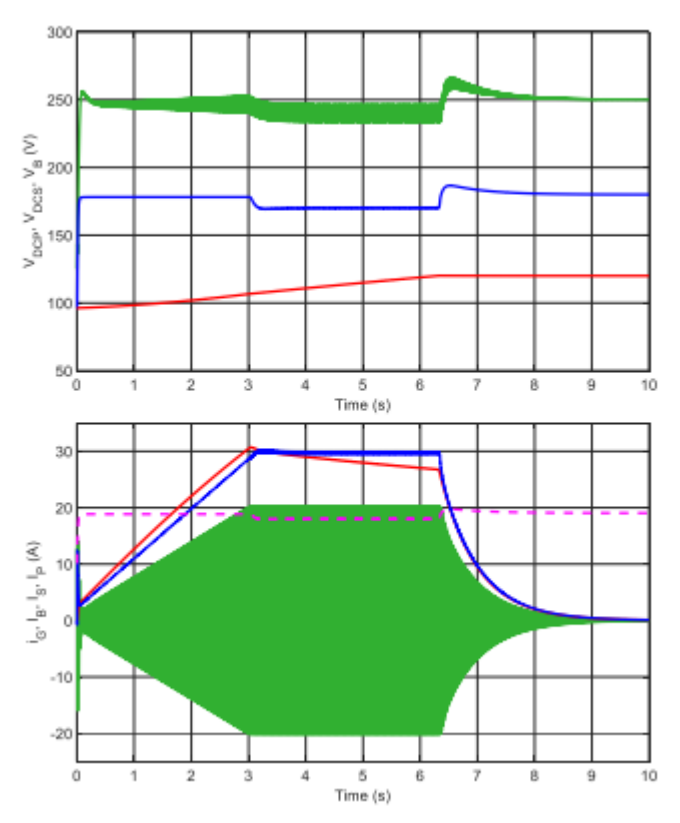


FIGURE 8. Top: VDCP voltage (with an offset of -200V) (green), VDCS (blue), VB (red). Bottom: iG (green), IS (blue), IB (red), IP (dashed magenta).

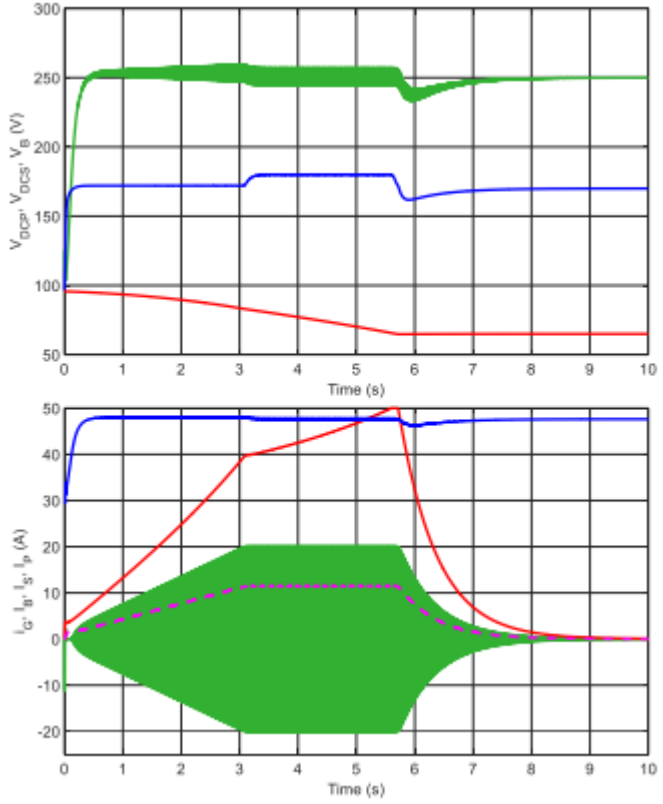


FIGURE 9. Top: VDCP voltage (with an offset of -200V) (green), VDCS (blue), VB (red). Bottom: iG (green), IS (blue), IB (red), IP (dashed magenta).



DOI: 10.17148/IJIREEICE.2025.131020

The behavior of the primary quantities involved in the battery charging process is illustrated in Fig. 41. Specifically, it pertains to the procedure that elevates the voltage across the capacitor Ceq from VB,N to VB,M. Concurrently, the charging of the capacitors CDCP and CDCS is also executed, raising them to their designated working voltage. The upper section of Fig. 41 displays the voltage across CDCP in green. To enhance the clarity of the figure, an offset has been applied to VDCP prior to graphing, necessitating the addition of 200 V to the plotted value to ascertain its actual measurement. The blue line denotes VDCS, while the red line signifies VB. The lower section of Fig. 41 illustrates the current iG in green, the current amplitude IS in blue, and the current IB in red. The magenta dotted line indicates the amplitude IP, calculated by where VHFP represents the amplitude of the first harmonic component of vHFP. Upon examining the figure, numerous behaviors previously discussed in earlier sections can be identified. The initial charging of CDCP and CDCS occurs at a significantly faster rate compared to that of the battery, allowing their voltage to be consistently regarded as being in a steady state. Following the charging of CDCP, the amplitudes IG and IS continue to increase, as outlined in subsection IV-C2. The rise in IS suggests that a growing power PPS is being transferred to the secondary section of the BWV2H, thereby elevating the voltage VDCS. This effect is counterbalanced by the rise in IB, which injects an ever-increasing power into the battery.

After approximately 3 seconds, once the maximum grid power is attained, the output of CVDCP,PG(s) is constrained, and the amplitude of iG stabilizes. This alteration in the slope of IG is not immediately mirrored by IS, which continues to rise for a brief moment. This results in a reduction of VDCP voltage as the transferred power PPS surpasses the power PG extracted from the grid. This reduction indicates that AL_VDCP_C, via CVDCP,PPS(s), diminishes PPS,ref, and, as a result, IS,ref. The decrease in transferred power is not promptly observed in the secondary section of the BWV2H. Consequently, the equilibrium between iS, which charges CDCS, and IB, which discharges it by transferring power to the battery, is momentarily disrupted. This occurrence leads to a decline in VDCS, to which AL_VDCS_B responds through CVDCS,PB(s) by lowering PB,ref. A new balance is thus established in which VDCP and VDCS remain constant and near their lower references while the battery is charged with a constant power equal to the maximum available from the grid. As VB rises, IB gradually decreases to maintain PB at a constant level. This operational mode persists until 6.5 seconds after the system power is activated. At this moment, VB attains its end-of-charge value VB,M, and AL_VB_B, through CVB,PB(s), reduces PB,ref.

The examination of the behavior of IP and IS warrants specific considerations. The BWV2H discussed in this paper employs series-series compensation, such that, disregarding the resistive voltage drops across the coils and the resonance capacitors, when the system effectively transfers power, the first harmonic component of vHFP corresponds to the voltage induced across the primary coil by iS. As a result, the first harmonic amplitude VHFP of vHFP is directly proportional to IS. Given that the HFSC is not regulated during battery charging, VHFS is proportional to VDCS and remains nearly constant throughout the entire charging process.

To adjust PPS, it is essential to manipulate IS by influencing VHFP. This condition elucidates why the waveform of IS mirrors that of IB, which is approximately proportional to PPS. Conversely, there is no direct correlation between VHFP and IP, as, considering the symmetry in the operation of the coupled coils, the latter is proportional to VHFS and thus remains almost constant. This behavior does not contradict the observation that at the conclusion of the charging process, the transferred power is nearly zero. Under these circumstances, IB approaches zero, and the equivalent load observed at the terminals of the series of the secondary coil and its resonant capacitor behaves almost like an open circuit. Consequently, the primary coil functions as if there were no coupling between the two sections of the BWV2H. The impedance presented by the series of the primary coil and its resonance capacitor is ideally zero, and thus a voltage vHFP with a very small first harmonic amplitude suffices to keep IP at a value significantly above zero.

The battery discharge process from voltage VB,N to VB,m is illustrated in Fig. 42. According to the conventions of Fig. 2, the current IB is always negative since it discharges the battery. However, in Fig. 42 its sign has been changed to facilitate comparison with the other currents. The current iG is represented by the green line, and the amplitude IP by the dashed magenta line. In this case, symmetrically to what has been explained in the previous subsection about IP, IS is not a controlled quantity and has been computed from PSP and VHFS using an equation similar to (42). It is represented in Fig. 42 by the blue line. From the comparison between Figs. 41 and 42 it is possible to recognize many similarities between the charging and discharging processes. In this case also, the initial charge of CDCP and CDCS is very fast compared to the discharge of the battery, so their voltages can be considered always in steady state. After loading CDCS, AL_VDCS_B and AL_VDCS_D interact in order to ramp up the power PB extracted from the battery and the power PSR transmitted to the primary section of the BWV2H while at the same time maintaining VDCS between its higher and lower reference. This behavior is highlighted in the figure by the ramp trend of the current IB and of the amplitude IP. In the primary section, the received power PSP charges CDCP increasing VDCP but this effect is opposed by AL_VDCP_B which reacts by acting on IG,ref to increase the power injected into the grid. At a first glance, no difference is visible between the waveforms of



DOI: 10.17148/IJIREEICE.2025.131020

iG shown in Figs. 41 and 42, but in the latter case iG is in phase opposition to vG while in the former case they are inphase. Approximately 3 s after switching on the system, the maximum power that can be injected into the grid is reached, so the output of CVDCP,PG(s) is limited and IG remains constant.

The alteration in the slope of PG is not immediately mirrored on PB, which consequently charges CDCS to a voltage that is nearly equal to VDCS, ref, high. The AL VDCS B algorithm responds by decreasing PB, ref to prevent a further rise in VDCS. This measure leads to the formation of a cusp on the IB graph. From this moment onward, the battery discharges at a steady power level, resulting in an increase in IB as VB diminishes. Approximately 5.7 seconds into the simulation, for a brief period, the absolute value of IB, ref is capped at its peak value of 50 A. However, shortly thereafter, VB reaches its end-of-discharge threshold, VB,min, leading to a reduction in the current discharging from the battery. This results in a decrease in the current charging CDCS, causing VDCS to drop until AL_VDCS_D lowers PSP,ref, thereby restoring equilibrium and keeping VDCS stable. The decline in power from the secondary section results in a reduction in VDCP, which is counterbalanced by AL_VDCP_B, leading to a decrease in IG. From this point forward, the battery continues to discharge at a constant voltage, resulting in a decrease in the amplitude of IB that follows an approximately hyperbolic trajectory. A similar trend is observed in the power exchanged between the two sections of BWV2H and the grid, as evidenced by the profiles of IG and IP. The amplitude IS remains relatively constant throughout the process. This behavior can be explained symmetrically to the observations made regarding IP in the preceding subsection. During the battery discharge, the first harmonic component of vHFP compensates for the voltage induced across the primary coil by the current iS. Given that the HFPC functions as a diode rectifier, VHFP is directly proportional to VDCP and adheres to its profile, resulting in IS being nearly constant with only minor fluctuations corresponding to those of VDCP.

V. CONCLUSION

This document addresses the development of a control strategy for a wireless battery charger system featuring V2H functionality. The proposed strategy focuses on managing the voltages of the DC buses and the battery. This is achieved by adjusting the power exchanged between the grid and the battery via static power converters and coupled coils. Such an approach ensures that the charging and discharging needs of the battery are met without surpassing the voltage or current limits of the converters. Concurrently, the requirements for grid power exchange are fulfilled. The control strategy is structured into two levels. The algorithms at the internal level handle the current references and feedback signals obtained from the BWV2H circuits to produce gate commands for the static converters. Meanwhile, the external level algorithms create the references for the power to be exchanged among the various stages and between the two sections of the BWV2H. The necessity to integrate the operations of the different stages prompted the creation of interactive control algorithms. Their interaction facilitates a smooth transition from one operating condition to another, such as shifting from constant current charging to constant voltage charging, without requiring any information exchange between them. The information exchange between the two sections of the BWV2H is restricted to a single reference and one error quantity during both the charging and discharging phases of the battery. The operation of the internal level algorithms has been validated in the Simulink environment using precise circuit models of the power converters that make up the BWV2H. To minimize execution time, the operations of the external level algorithms have been simulated using time-average models of the converters. The analysis of the simulation results verifies the proper functioning of all algorithms. Ultimately, the entire control strategy has been implemented in a simulation model and tested during both the charging and discharging processes.

REFERENCES

- [1]. International Energy Agency (IEA). Global EV Outlook 2021. Accessed: Jun. 17, 2023. [Online]. Available: https://iea.blob.core.windows.net/assets/ed5f4484-f556-4110-8c5c-4ede8bcba637/GlobalEVOutlook 2021.pdf
- [2]. M. Bertoluzzo, S. Giacomuzzi, and A. Kumar, "Design of a bidirectional wireless power transfer system for vehicle-to-home applications," Vehicles, vol. 3, no. 3, pp. 406–425, Jul. 2021.
- [3]. A. Kumar and N. Neogi, "Bidirectional converter and energy storage system," Int. J. Enhanced Res. Sci. Technol. Eng., vol. 4, no. 6, pp. 15–23, 2015.
- [4]. D. Patil, M. K. McDonough, J. M. Miller, B. Fahimi, and P. T. Balsara, "Wireless power transfer for vehicular applications: Overview and challenges," IEEE Trans. Transport. Electrific., vol. 4, no. 1, pp. 3–37, Mar. 2018.
- [5]. G. Buja, R. K. Jha, M. Bertoluzzo, and M. K. Naik, "Analysis and comparison of two wireless battery charger arrangements for electric vehicles," Chin. J. Electr. Eng., vol. 1, no. 1, pp. 50–57, Dec. 2015.
- [6]. European Commission. (1999). 1999/519/EC: Council Recommendation of 12 July 1999 on the Limitation of Exposure of the General Public to Electromagnetic Fields (0 Hz to 300 GHz). Accessed: Jun. 17, 2023. [Online]. Available: https://eur-lex.europa.eu/legal-content/EN/TXT/ HTML/?uri=CELEX:31999H0519&from=IT



IJIREEICE

International Journal of Innovative Research in Electrical, Electronics, Instrumentation and Control Engineering Impact Factor 8.414 Refereed journal Vol. 13, Issue 10, October 2025

DOI: 10.17148/IJIREEICE.2025.131020

- [7]. R. Dai, R. Mai, Z. Zhu, and Z. He, "Time-weighted average efficiency optimization for reconfigurable IPT system with CC and CV outputs," in Proc. IEEE Energy Convers. Congr. Expo. (ECCE), Baltimore, MD, USA, Sep. 2019, pp. 117–120.
- [8]. M. Bertoluzzo, P. D. Barba, M. Forzan, M. E. Mognaschi, and E. Sieni, "Field models for the electromagnetic compatibility of wireless power transfer systems for electric vehicles," Eng. Comput., vol. 39, no. 7, pp. 2802–2819, 2022.
- [9]. U. Vuyyuru, S. Maiti, and C. Chakraborty, "Active power flow control between DC microgrids," IEEE Trans. Smart Grid, vol. 10, no. 5, pp. 5712–5723, Sep. 2019.
- [10]. P. He and A. Khaligh, "Comprehensive analyses and comparison of 1 kW isolated DC–DC converters for bidirectional EV charging systems," IEEE Trans. Transport. Electrific., vol. 3, no. 1, pp. 147–156, Mar. 2017.
- [11]. Z. H. Shi, Z. C. Qiu, X. Y. Chen, and M. Y. Li, "Modeling and experimental verification of bidirectional wireless power transfer," IEEE Trans. Appl. Supercond., vol. 29, no. 2, pp. 1–5, Mar. 2019.
- [12]. F. Liu, K. Li, K. Chen, and Z. Zhao, "A phase synchronization technique based on perturbation and observation for bidirectional wireless power transfer system," IEEE J. Emerg. Sel. Topics Power Electron., vol. 8, no. 2, pp. 1287–1297, Jun. 2020.
- [13]. D. Dong, I. Cvetkovic, D. Boroyevich, W. Zhang, R. Wang, and P. Mattavelli, "Grid-interface bidirectional converter for residential DC distribution systems—Part one: High-density two-stage topology," IEEE Trans. Power Electron., vol. 28, no. 4, pp. 1655–1666, Apr. 2013.
- [14]. C. A. Hill, M. C. Such, D. Chen, J. Gonzalez, and W. M. Grady, "Battery energy storage for enabling integration of distributed solar power generation," IEEE Trans. Smart Grid, vol. 3, no. 2, pp. 850–857, Jun. 2012.
- [15]. M. Tabari and A. Yazdani, "Stability of a DC distribution system for power system integration of plug-in hybrid electric vehicles," IEEE Trans. Smart Grid, vol. 5, no. 5, pp. 2564–2573, Sep. 2014.
- [16]. G. Delille, B. Francois, and G. Malarange, "Dynamic frequency control support by energy storage to reduce the impact of wind and solar generation on isolated power system's inertia," IEEE Trans. Sustain. Energy, vol. 3, no. 4, pp. 931–939, Oct. 2012.
- [17]. V. Monteiro, J. G. Pinto, and J. L. Afonso, "Operation modes for the electric vehicle in smart grids and smart homes: Present and proposed modes," IEEE Trans. Veh. Technol., vol. 65, no. 3, pp. 1007–1020, Mar. 2016.
- [18]. C. Liu, K. T. Chau, D. Wu, and S. Gao, "Opportunities and challenges of vehicle-to-home, vehicle-to-vehicle, and vehicle-to-grid technologies," Proc. IEEE, vol. 101, no. 11, pp. 2409–2427, Nov. 2013.
- [19]. V. Monteiro, B. Exposto, J. C. Ferreira, and J. L. Afonso, "Improved vehicle-to-home (iV2H) operation mode: Experimental analysis of the electric vehicle as off-line UPS," IEEE Trans. Smart Grid, vol. 8, no. 6, pp. 2702–2711, Nov. 2017.
- [20]. W. L. Malan, D. M. Vilathgamuwa, and G. R. Walker, "Modeling and control of a resonant dual active bridge with a tuned CLLC network," IEEE Trans. Power Electron., vol. 31, no. 10, pp. 7297–7310, Oct. 2016.
- [21]. L. Wang, U. K. Madawala, and M.-C. Wong, "A wireless vehicle-to-gridto-home power interface with an adaptive DC link," IEEE J. Emerg. Sel. Topics Power Electron., vol. 9, no. 2, pp. 2373–2383, Apr. 2021.
- [22]. J. M. Miller, O. C. Onar, and M. Chinthavali, "Primary-side power flow control of wireless power transfer for electric vehicle charging," IEEE J. Emerg. Sel. Topics Power Electron., vol. 3, no. 1, pp. 147–162, Mar. 2015.
- [23]. W. Shi, J. Deng, Z. Wang, and X. Cheng, "The start-up dynamic analysis and one cycle control-PD control combined strategy for primaryside controlled wireless power transfer system," IEEE Access, vol. 6, pp. 14439–14450, 2018.
- [24]. B. Vardani and N. R. Tummuru, "A single-stage bidirectional inductive power transfer system with closed-loop current control strategy," IEEE Trans. Transport. Electrific., vol. 6, no. 3, pp. 948–957, Sep. 2020.
- [25]. T. Tan, K. Chen, Y. Jiang, Q. Lin, L. Yuan, and Z. Zhao, "A bidirectional wireless power transfer system control strategy independent of real-time wireless communication," IEEE Trans. Ind. Appl., vol. 56, no. 2, pp. 1587–1598, Mar./Apr. 2020.
- [26]. A. Sangswang and M. Konghirun, "Optimal strategies in home energy management system integrating solar power, energy storage, and vehicleto-grid for grid support and energy efficiency," IEEE Trans. Ind. Appl., vol. 56, no. 5, pp. 5716–5728, Sep. 2020.
- [27]. N. Mukaiyama, H. Omeri, N. Kimura, T. Morizane, M. Tsuno, and M. Nakaoka, "A novel type of bidirectional IPT with a dual-active seamless controlled single-ended converter for wireless V2H," in Proc. 19th Int. Conf. Electr. Drives Power Electron. (EDPE), Dubrovnik, Croatia, Oct. 2017, pp. 53–58.
- [28]. R. Ishii, H. Omori, M. Tsuno, T. Morizane, and H. Matayoshi, "An improvement of power control and transfer efficiency in a singleended converter driven WV2H by a new control scheme," in Proc. 3rd Int. Conf. Electr., Control Instrum. Eng. (ICECIE), Kuala Lumpur, Malaysia, Nov. 2021, pp. 1–6.
- [29]. A. A. S. Mohamed, T. Youssef, and O. Mohammed, "Vehicle side predictive power-flow control of bidirectional WPT system for EV ancillary services," in Proc. IEEE Appl. Power Electron. Conf. Expo. (APEC), Tampa, FL, USA, Mar. 2017, pp. 3211–3217.



IJIREEICE

International Journal of Innovative Research in Electrical, Electronics, Instrumentation and Control Engineering
Impact Factor 8.414

Refereed journal

Vol. 13, Issue 10, October 2025

DOI: 10.17148/IJIREEICE.2025.131020

- [30]. X. Liu, Y. Wang, H. Chen, J. Mai, and D. Xu, "A bidirectional WPT system using double-sided LCC compensation topology and full-bridge active rectifier," in Proc. IEEE Transp. Electrific. Conf. Expo, Asia—Pacific (ITEC Asia—Pacific), Haining, China, Oct. 2022, pp. 1–7.
- [31]. G. Pandey and T. N. Reddy, "Power flow study of grid connected bidirectional WPT systems for EV application," in Proc. IEEE Int. Conf. Power Electron., Smart Grid Renew. Energy (PESGRE), Kochi, India, Jan. 2020, pp. 1–6.
- [32]. A. Singhal and N. R. Tummuru, "Bidirectional power flow control of single phase matrix converter based inductive WPT system for e-vehicle applications," in Proc. IEEE 10th Power India Int. Conf. (PIICON), New Delhi, India, Nov. 2022, pp. 1–6.
- [33]. L. Wang, W. Tian, U. K. Madawala, and J. Yang, "A power selective control of versatile wireless vehicle-grid-home power interface (VW-VGH-PI)," in Proc. IEEE Southern Power Electron. Conf. (SPEC), Kigali, Rwanda, Dec. 2021, pp. 1–5.
- [34]. Wireless Power Transfer for Light-Duty Plug-In/Electric Vehicles and Alignment Methodology, Standard J2954, SAE International, 2020.
- [35]. Reference Technical Rules for the Connection of Active and Passive Users to the LV Electrical Utilities, Standard CEI 0-21, Italian Electrotechnical Committee (CEI), 2019. Accessed: Jun. 17, 2023. [Online]. Available: https://www.ceinorme.it/it/norme-cei-0-16-e-0-21.html
- [36]. M. H. Rashid, Power Electronics: Devices, Circuits and Applications, 3rd ed. London, U.K.: Pearson, 2004.
- [37]. R. K. Jha, G. Buja, M. Bertoluzzo, S. Giacomuzzi, and K. N. Mude, "Performance comparison of the one-element resonant EV wireless battery chargers," IEEE Trans. Ind. Appl., vol. 54, no. 3, pp. 2471–2482, May 2018.
- [38]. M. Bertoluzzo, S. Giacomuzzi, and M. Forato, "Performance analysis of envelope modelling applied to resonant converters," IEEE Trans. Ind. Electron., vol. 69, no. 4, pp. 4046–4055, Apr. 2022.
- [39]. N. Das, A. Haque, H. Zaman, S. Morsalin, and S. Islam, "Domestic load management with coordinated photovoltaics, battery storage and electric vehicle operation," IEEE Access, vol. 11, pp. 12075–12087, 2023.
- [40]. A. Mohammad, M. Zuhaib, I. Ashraf, M. Alsultan, S. Ahmad, A. Sarwar, and M. Abdollahian, "Integration of electric vehicles and energy storage system in home energy management system with home to grid capability," Energies, vol. 14, no. 24, p. 8557, Dec. 2021.